Quantification of Systolic Count Increase in Technetium-99m-MIBI Gated Myocardial SPECT

Kazuki Fukuchi, Toshiisa Uehara, Takakazu Morozumi, Eiichiro Tsujimura, Shinji Hasegawa, Kenji Yutani, Hideo Kusuoka and Tsunehiko Nishimura

Division of Tracer Kinetics, Biomedical Research Center, and Department of First Internal Medicine, Osaka University Medical School, Suita, Osaka, Japan

This study was performed to clarify the validity of quantification of myocardial wall thickening by the count increase method using electrocardiography (ECG)-gated SPECT. **Methods:** We performed a phantom study to examine the quantification of this method and to clarify the relationship between the changes of relative counts and objective size (such as myocardial wall) under various conditions. In addition, in volunteers, the percent count increase (%CI) was analyzed in left ventricular segments based on circumferential profile curve analysis by ECG-gated SPECT with ^{99m}Tc-MIBI (methoxy-isobutyl-isonitrile), and it was compared with the regional systolic wall thickness (%Th) assessed by echocardiography during low-dose dobutamine infusion. **Results:** In our phantom study, the relative count changes were correlated linearly with the object size only within less than 20 mm. Recovery coefficient curves were influenced by acquisition parameters such as type of collimator, diameter of camera rotation, counts and photon scattering. In ECG-gated SPECT, the %CI value was increased gradually at each stage after dobutamine infusion, in relation to the increase of the %Th seen on echocardiography, although there are significant large deviations between these two parameters. **Conclusion:** In this study, quantitative analysis based on the %CI in ECG-gated SPECT may underestimate regional wall thickening. These data should be considered in the evaluation of the %CI as an index of myocardial function.

Key Words: ECG-gated SPECT; technetium-99m-MIBI

J Nucl Med 1997; 38:1067–1073

Electrocardiography (ECG)-gated myocardial SPECT using ^{99m}Tc-labeled methoxy-isobutyl-isonitrile (MIBI) provides the opportunity to assess both regional myocardial perfusion and function within a single study (*1*). Because of the relatively low spatial resolution of SPECT perfusion imaging, the count density is linearly related to the increase in wall thickness during myocardial contraction (*2*). This approach is valid because of the partial volume effect. A change in the size of an object (such as the myocardial wall) results in a change in its apparent concentration of counts (brightness), when the size of the object is less than twice the resolution of the gamma camera (*3,4*). The usefulness of this count density method to evaluate regional myocardial wall thickening has been reported (*5–7*); however, the quantification has not been established.

To clarify the validity of quantification of wall thickening by the count increase method using ECG-gated SPECT, we performed a phantom study to investigate the relationship between relative counts and objective size under various conditions. In addition, ECG-gated SPECT was performed in normal male volunteers during low dose dobutamine infusion to obtain sequential changes of regional myocardial count accompanied by various myocardial wall thickness.

Received Jun. 17, 1996; revision accepted Nov. 13, 1996.

For correspondence or reprints contact: Kazuki Fukuchi, MD, PhD (correspondence) or Tsunehiko Nishimura, MD, PhD (reprints), Division of Tracer Kinetics, Biomedical Research Center, Osaka University Medical School, Yamada-oka, 2-2 Suita, Osaka, 565 Japan.

MATERIALS AND METHODS

Phantom Study

For in vitro comparison, a phantom formed by two eccentric cylinders of Plexiglas, simulating the myocardial wall, was used (Fig. 1A) (*2,4*). The volume between the two cylinders was filled with a homogeneous solution of 0.25 MBq/ml of ^{99m}Tc. This phantom, simulating myocardial wall with variable thickness, allows the evaluation of object size in the range from 0 to 40 mm. In some trials, the phantom was placed in a water-filled pool to represent soft tissue. It was placed on the imaging table so that it was located on the center of rotation of the detector system. Image acquisitions were performed using a three-headed rotating gamma camera system [GCA9300A/HG, Toshiba Medical Co., Tokyo, Japan (*8*)] with 120° × 3 (20 steps) using the 24% main window centered at ^{99m}Tc photopeak energy (140 KeV) and the 3% subwindow on both sides of the main window (triple-energy window) to be able to use scatter correlation (*9*).

Data Acquisition. Image acquisitions were performed under various parameters such as type of collimator, diameter of camera rotation, counts, matrices sizes and with or without correction of scattering. At first, two types of collimators (low-energy general-purpose collimators and low-energy high resolution collimators) were used to simulate patient data acquisition. Effective resolution at full-width half maximum of low-energy general purpose (LEGP) collimators was 17.5 mm in the axial direction, and that of low-energy high resolution (LEHR) collimators was 13.0 mm. The measurement of camera resolution was performed according to National Electrical Manufacturers Association standards (*10*). These data were acquired using 64 × 64 matrix size, 40 sec/step and 210 mm of angle of rotation-to-detector distance without scatter correction. Second, difference in angle of rotation-to-detector distances (at 210 mm and at 307 mm diameter) were adapted using the LEGP collimators, 64 × 64 matrix size, 40 sec/step without scatter correction. Third, differences in acquisition time using 40 sec/step and 10 sec/step were performed with the LEGP collimators, 64 × 64 matrix size, 210 mm of rotation and without scatter correction. Fourth, two matrices sizes (64 × 64 and 128 × 128) were performed with the LEGP collimators, 40 sec/step, 210 mm of rotation without scatter correction. Fifth, correction of Compton scatter compensation using the triple-energy window method was performed for the phantom, which was placed in the water-filled container using the LEGP collimator, with 64 × 64 matrix size, 40 sec/step and 210 mm of rotation.

In each experimental condition, acquisition trials were performed five times, and the average value was obtained.

Data Processing. The projections were reconstructed using Shepp–Logan filtered backprojection, and the contribution from high frequency noise was decreased with prereconstruction Butter-

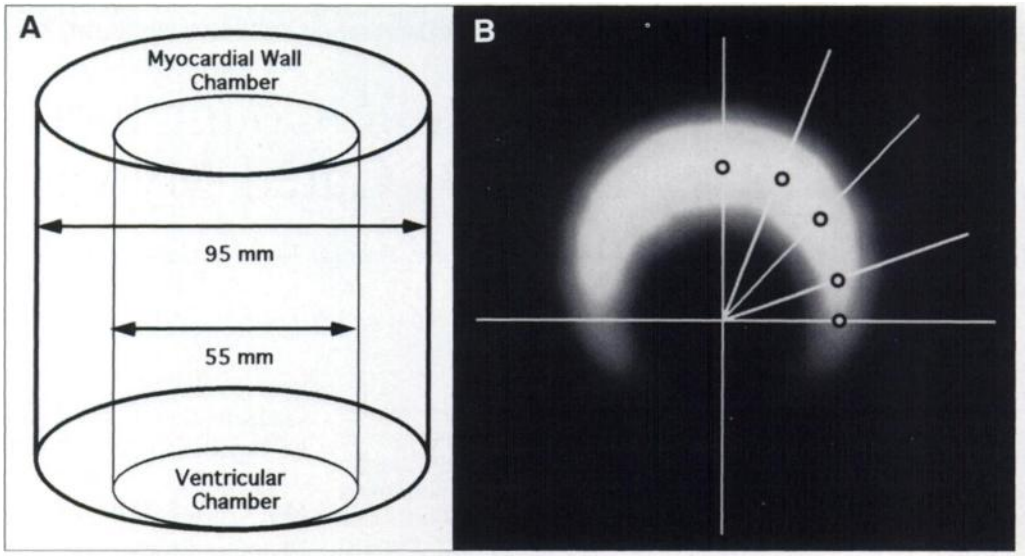

FIGURE 1. (A) Scheme of the phantom. The chamber was filled with a solution of ^{99m}Tc and simulated myocardial thickness over a broad range of values (from 0 to 40 mm). (B) Scheme of circumferential profile analysis.

worth filtering (cutoff = 0.28 cycle/pixel, power factor = 8). The data were reconstructed so that the long axes of the phantoms were perpendicular to the line through the center of rotation. Quantitative analysis was performed on each of the short axis slices (Fig. 1B). Each short axis slice was subjected to a maximal count circumferential profile analysis similar to that performed in quantitative analysis of thallium SPECT data (*11,12*). For all slices, the maximum count was determined along 36 radial vectors (i.e., 10° angular increments), which emanated from an operator-defined center of the inner cylinder. In our analysis program, the profile was reconstructed down to the values of 16 radii spaced at 22.5° intervals, and mean value of the relative counts of the region was expressed as the percentage of the maximum count of 16 regions of the short-axis slice. From the measurement of true myocardial wall chamber thickness at 22.5° angular intervals from the phantom and the relative count at the center of the wall chamber in the mid-level of the phantom, the recovery coefficients (RC) were evaluated (*3*). Estimation of the RC was performed on a personal computer by a nonlinear least-squares curve-fitting procedure. The goodness-of-fit was evaluated by Akaike's information criterion (*13*).

Simulation. To investigate the theoretical relationship between percent count increase (%CI) and percent wall thickening (%Th) obtained from the phantom, we performed the following simulation study. The RC curve was mathematically generated using the fitting algorithm, which was obtained earlier (SPECT acquisition was performed using the LEGP collimators, 64 × 64 matrix, 210 mm of rotation, 40 sec/step without scatter correction). The %Th was calculated as: [(x − the initial width)/the initial width] × 100, and the %CI was calculated as: [(y − the initial counts)/the initial counts] × 100, where x, y is a certain thickness and counts. This simulation was performed for the initial myocardial width of 5, 10 and 15 mm.

ECG-Gated SPECT and Echocardiography During Dobutamine Infusion

Study Protocol. Four normal male volunteers (mean age, 28 ± 3 yr old) were studied. Informed consent was obtained from each subject, and the study was performed according to the standard ethical guidelines of the Osaka University Medical School. Technetium-99m-MIBI was prepared according to the manufacturer's recommendations, and a 740-MBq dose was administered by intravenous injection. Approximately 1 hr after ^{99m}Tc-MIBI administration, echocardiography and ECG-gated SPECT at rest and pharmacological stress protocol were performed to assess dobutamine-induced myocardial wall thickening. The stages of the dobutamine protocol were rest (baseline), 1 μg/kg/min and 3 μg/kg/min, respectively. Dobutamine was administered intravenously using a digital perfusion pump under continuous ECG monitoring. Beginning 5 min after the start of each stage, echocardiography and subsequent SPECT acquisition were performed. Blood pressure was recorded at the end of each stress stage.

Measurement of Myocardial Wall Thickening. Two-dimensional echocardiography was performed with commercially available equipment with a phase array system (SONULAYER SSA-270A, Toshiba Medical Co., Tokyo, Japan). All of the echocardiographic studies were performed by a single experienced cardiologist. At rest and at each stage of the infusion, cardiac views were continuously recorded on videotape. During the echocardiographic study, the operator was asked to identify proximal to distal short-axis, long-axis and apical two- or four-chamber views. The left ventricular wall thickening was measured at the midpapillary muscle short-axis level. Endocardial and epicardial borders were manually generated, and average values for myocardial wall thickness were measured. As the echocardiographic index of myocardial wall thickening, the regional %Th was calculated as: [(ThES − ThED)/ThED] × 100, where ThES is the thickness at end-systole and ThED is the thickness at end-diastole (in millimeters) (*14,15*).

Measurement of Myocardial Count Increase. ECG-gated SPECT acquisition was performed in 20 steps (90 sec/step), 120° × 3 with a 64 × 64 matrix using the same gamma camera system. At each projection, a total of 10 individual ECG-gated frames/cardiac cycle was acquired. With the equipped computer system (GMS-550A, Toshiba Medical Co., Tokyo, Japan), transaxial tomograms were reconstructed from the projection data using Shepp–Logan filtered backprojection with use of prereconstruction Butterworth filtering (cutoff = 0.28 cycle/pixel, power factor = 8), and they were then reoriented along cardiac planes. As the ECG-gated SPECT index of myocardial wall thickening, the regional %CI was analyzed. The end-diastolic (ED) phase was identified at the beginning of the R-wave (the first frame), and the end-systolic (ES) phase was defined as the frame having the maximum count among 10 divided cardiac cycles (usually, the third or fourth frame). From the two images of ED and ES phase, the midventricular portions of short-axis slices were selected using a reference of the vertical long-axis image. The processing area was surrounded by a circular region of interest to exclude hepatic and diaphragmatic activity, and the center of the short-axis myocardium was determined manually. The maximum count was determined along 40 radial vectors. The extracted profile curve provides information on the distribution of MIBI in the myocardium. All the profiles were displayed in two-dimensional polar coordinates, which effectively

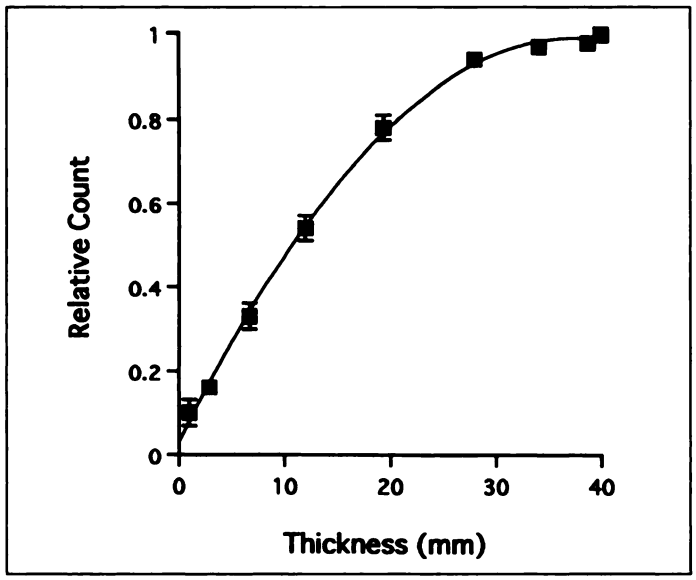

FIGURE 2. Plot of RC versus object size (GP collimator, 64 × 64 matrix, 210 mm of rotation, 40 sec/step and without scatter correction).

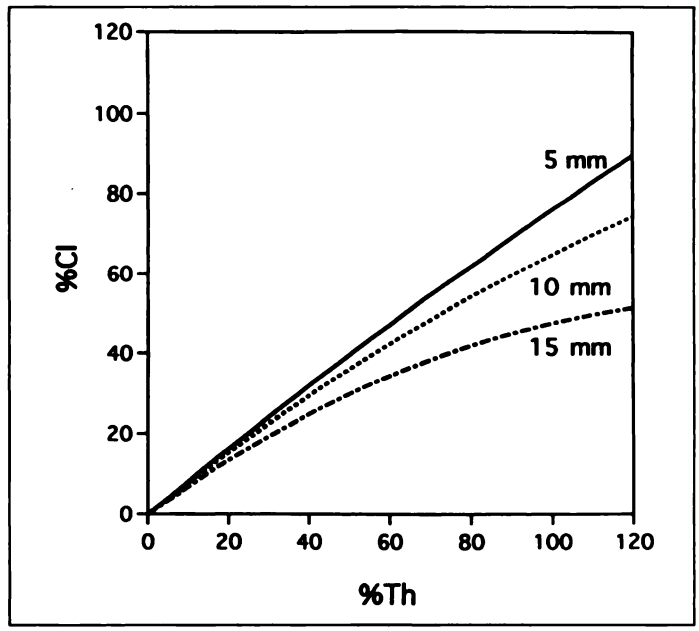

FIGURE 3. Correlation between %CI and %Th of the phantom with varied initial myocardial wall width in the simulation.

ties the 0° and 360° ends of the array together. Each bull's-eye image was divided into 12 segments (4 sectors with 3 depths from apex to base) for quantitative analysis. The regional %CI images were constructed using the actual counts in ES and ED polar maps. The %CI was calculated as: [(ES − ED pixel counts)/ED pixel counts] × 100 (%) (*16*).

In this study, regional matching of two modalities and correlation between the %Th and the %CI was performed in the anterior wall, septal wall, inferior wall and lateral wall, respectively. Care was taken to ensure that echocardiography and ECG-gated SPECT data were obtained from similar regions. The left ventricular segmental anatomy was graded using standard nomenclature in both of the two modalities (*11,17*), and we performed matching of regional myocardial segments.

Statistical Analysis

Data are expressed as the mean ± 1 s.d. Comparisons among groups were performed with the paired Student's t-test. Correlations were determined by linear regression analysis. Probability values less than 0.05 were considered as significant.

RESULTS

Phantom Study

The RC curves from the phantom study (with LEGP, 64 × 64 matrix size, 210 mm of rotation, 40 sec/step and without scatter correction) are shown in Figure 2. Although all parts of the object have the same radioactive concentration, the part with the smaller thickness shows lower concentration of radioactivity. Relative counts showed a linear relationship with the object size for less than 20 mm thickness. In the simulation, the %CI and the %Th has a good correlation when the initial myocardial wall width is 5 mm. However, when the initial wall width is 10 or 15 mm in thickness, the two did not have a correlation, and the %CI tended to be lower than the %Th, especially in the segments where the %Th was high (Fig. 3).

Figure 4A shows RC curves obtained using the two different collimators. Measured data primarily reflect the differences in the geometrical spatial resolution of the two collimators. Good correlation was observed between the object size and relative counts when the LEGP collimator was used. On the other hand, the RC curve deviated to the direction of weak partial volume effect significantly at object size of up to 20 mm when the LEHR collimator was used ($p < 0.005$). The influence of the diameter of the camera rotation differed with the collimator used. When the LEGP collimator was used, no significant difference was observed for the RC curves between 210 and 307 mm in the camera rotation diameter (Fig. 4B). On the other hand, when the LEHR collimator was used, the RC curves were quite different at 210 mm and at 307 mm diameter (Fig. 4C). At 307 mm rotation diameter, the RC curve was significantly deviated to the direction of emphasis of partial volume effect ($p < 0.005$).

Figure 5A shows the RC curves when the data acquisition times were different (one step for 40 sec and 10 sec). There was significant difference between the curves in 10–20 mm thickness when the data acquisition time was shorter (10 sec/step), and a weak correlation was observed between the object size and count. Figure 5B shows the RC curves at different matrix sizes. There was no significant difference between the curves acquired at 64 × 64 matrix size and at the 128 × 128 matrix size. When the phantom was placed or not placed in the water-filled container, the two RC curves showed quite different patterns (Fig. 5C). When the phantom was placed in the container, the partial volume effect was significantly weaker than that without the container ($p < 0.005$). The triple-energy window method (*9*) was performed to correct Compton scatter compensation in the phantom in the container, but little variation was observed.

Table 1 summarizes the optimum polynomial fitting parameters for each curve in phantom experiences.

ECG-Gated SPECT and Echocardiography During Dobutamine Infusion

In all volunteers, no perfusion abnormalities were shown in SPECT images in rest condition, respectively. The physiological changes during dobutamine infusion are shown in Table 2. No significant differences between each condition were found except in the diastolic blood pressure at baseline and that during 1 μg/kg/min dobutamine infusion ($p < 0.05$).

Images of ECG-gated SPECT and echocardiography of the same case are shown in Figure 6. The obvious change of myocardial wall thickening in dobutamine stress condition using echocardiography, however, in spite of the same condition, a little change was observed using ECG-gated SPECT.

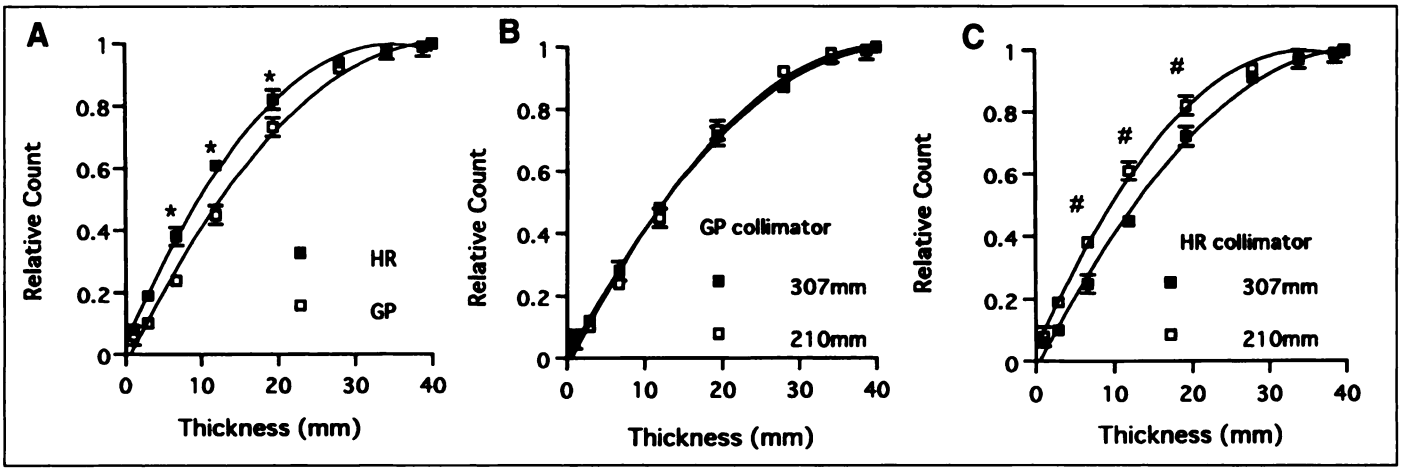

FIGURE 4. Plot of RC versus object size under various conditions. (A) The RC were obtained using the high resolution (HR) collimator or general purpose (GP) collimator. (B) The RC were obtained using the general purpose collimator (210 mm of rotation or 307 mm of rotation) and (C) the high resolution collimator. *p < 0.005, HR versus GP; #p < 0.005, 210 mm of rotation versus 307 mm of rotation.

The changes of regional %Th and %CI in each volunteer during dobutamine infusion are shown in Figure 7. In the quantitative analysis, the %Th increased accompanying the dose of dobutamine (rest, 45.6 ± 18.2; 1 μg/kg/min, 68.9 ± 17.6; and 3 μg/kg/min, 82.2 ± 26.4). There was a significant difference between the values at rest and during 3 μg/kg/min dobutamine ($p < 0.0001$). The %CI also increased with the dose of dobutamine (rest, 44.9 ± 6.5; 1 μg/kg/min, 50.7 ± 5.6; and 3 μg/kg/min, 54.0 ± 7.4). There was also significant difference between the %CI values at baseline and during 3 μg/kg/min dobutamine ($p < 0.0005$). However, the mean sequential change rate of %Th from rest to 3 μg/kg/min dobutamine was 1.88 ± 0.4, and that of %CI was 1.22 ± 0.2. There was a large difference between these change rates for these two parameters ($p < 0.0001$). The %CI was compared with the %Th in 44 segments at each condition (Fig. 8). Linear correlations between the two parameters were observed ($r = 0.62$, $p < 0.0005$); however, the slope and intercept of the regression line were quite different from the line of identity.

DISCUSSION

The current understanding of the relationship between count change and wall thickening follows from the work of Hoffman et al. (*3*) who showed that, for an object smaller than the resolution of the imaging system, the reconstructed count density is related to the size of the object. Our study focused on whether regional count changes of ECG-gated SPECT could be used as a means of identifying changes in myocardial wall thickness, that is, myocardial function (*2,7*).

Phantom Study

The RC curves from the phantom study did not indicate a linear relationship between object size and relative counts. These relationships are very important in the assessment of %CI quantitatively because the same %Th can give very different %CI, depending on the initial myocardial width. For example, under the same value of wall thickness change (ThES − ThED), when the value of ThED is sufficiently small, the %CI is not too far from the true %Th. When the ThED is large, in contrast, the %CI is smaller than the true %Th. In ECG-gated SPECT, however, the %CI is the reliable index of wall thickness because the values for baseline myocardial thickness were generally up to 10 mm in normal subjects. When the baseline myocardial thickness exceeded 10 mm, for example, in the case of hypertrophic cardiomyopathy, some corrections are clearly needed in the %CI according to the baseline myocardial thickness.

The RC curves were affected by the acquisition parameters such as the type of collimator, distance of camera rotation, total acquisition count and photon scattering. Marcassa et al. (*2*) discussed the possibility that this count density method has a limitation such as an increase in the background activity. Our results indicate not only the influence from background activity but also the other factors mentioned above. Clarke et al. (*18*)

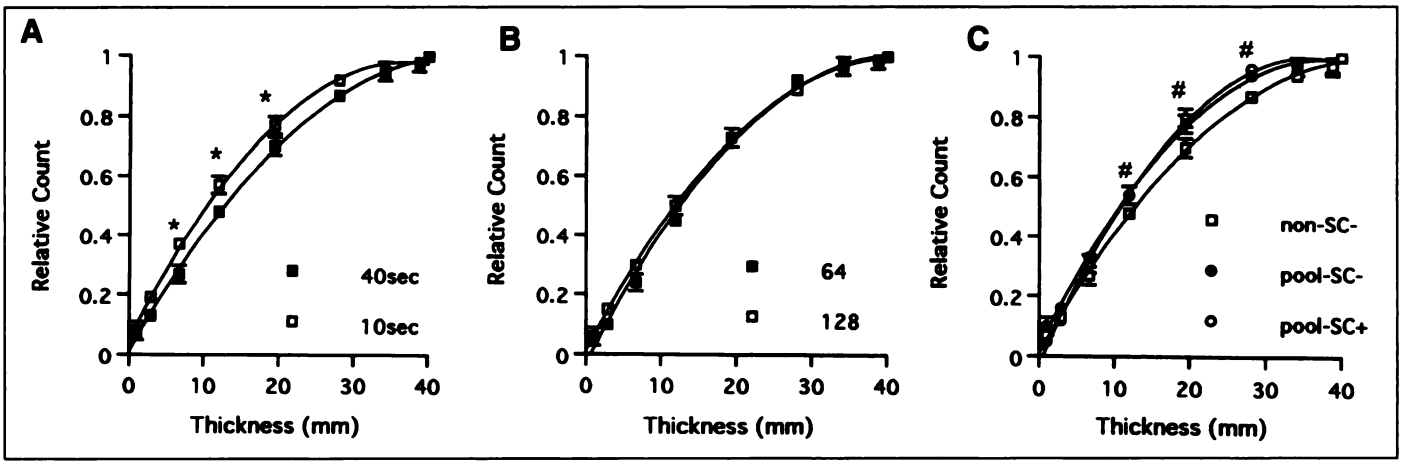

FIGURE 5. Plot of RC versus object size under various conditions. (A) A 40 sec acquisition or 10 sec acquisition, (B) a 64 × 64 matrix size or 128 × 128 matrix size and (C) background or not. *p < 0.005, 40 sec acquisition versus 10 sec acquisition; #p < 0.005, background versus not.

TABLE 1
Results of the Optimum Polynomial Fitting Parameters

Conditions	Parameter	
HR collimator	$Y = -0.0008X^2 + 0.0550X + 0.0413$	(Fig. 4A)
GP collimator	$Y = -0.0006X^2 + 0.050X - 0.0295$	
GP (307 mm)	$Y = 0.0005X^2 + 0.0469X + 0.0031$	(Fig. 4B)
GP (210 mm)	$Y = -0.0006X^2 + 0.0497X - 0.0295$	
HR (307 mm)	$Y = -0.0006X^2 + 0.0486X + 0.0232$	(Fig. 4C)
HR (210 mm)	$Y = -0.0008X^2 + 0.0550X + 0.0413$	
40 sec	$Y = -0.0005X^2 + 0.0449X + 0.0119$	(Fig. 5A)
10 sec	$Y = -0.0007X^2 + 0.0506X + 0.0489$	
64 × 64	$Y = -0.0006X^2 + 0.0497X - 0.0295$	(Fig. 5B)
128 × 128	$Y = -0.0006X^2 + 0.0478X + 0.0133$	
non-SC-	$Y = -0.0005X^2 + 0.0450X + 0.0113$	(Fig. 5C)
pool-SC-	$Y = -0.0007X^2 + 0.0513X + 0.0307$	
pool-SC+	$Y = -0.0008X^2 + 0.05738X + 0.0250$	

presented the results for the influence of various factors in the measurement of RC on source size in SPECT. The results of the phantom experiment indicate that several factors may operate for modification of the relationship between count density and thickness of the object such as camera resolution, signal/noise ratio and attenuation. The %CI values are influenced like the partial volume effect, and careful consideration is needed for the interpretation of %CI values. To obtain a good linear relationship between count and thickness in ECG-gated SPECT, the LEGP collimator is more suitable than the LEHR collimator, and adequate acquisition times (counts) are necessary. When the former typed collimator was used in our study, the RC curve was not deviated with the difference in the diameter of camera rotation.

Some limitations were considered in this phantom study. All SPECTs were acquired for 360° in this study but the majority of laboratories use 180°. The phantom that we used is not relevant to the myocardium, clinically. The particular numerical values of wall thickness at which we found a deviation from linearity of brightness versus thickness is specific to our camera, collimator and processing options. Other users with different equipment may experience similar phenomena but for greater or lesser wall thickness values. Some trials will be needed for the quantification of this count-based analysis, individually.

TABLE 2
Hemodynamic Parameters at Rest and During Dobutamine Infusion

Conditions	Heart rate	Blood pressure (systole/diastole)
Rest	78 ± 13	128 ± 3/75 ± 5
1 μg/kg/min	75 ± 14	143 ± 10/83 ± 3*
3 μg/kg/min	76 ± 10	158 ± 20/90 ± 9
Post stress	77 ± 6	147 ± 15/77 ± 6

*$p < 0.05$.
Heart rate values are expressed in beats per minute. Blood pressure values are expressed in mmHg.

ECG-Gated SPECT and Echocardiography During Dobutamine Infusion

Low dose dobutamine may be used as an alternative form of pharmacological stress, since it acts by an increase in coronary artery blood flow, oxygen demand and myocardial wall thickening. This allows an incremental protocol in which the dose of dobutamine is increased analogous to the workload in exercise stress testing without significant change of heart rate (*19*). Since the %CI of ECG-gated SPECT is increased in proportion to the increase of wall thickening in volunteers, the %CI is thought to be the reliable index of wall thickening in vivo. Nevertheless, compared to the actual %Th values which are measured by echocardiography in the same stress condition, the change of %CI was significantly smaller than that of %Th. Two-dimensional echocardiography is the only readily available noninvasive technique that allows quantitative analysis of wall thickening around the entire left ventricular circumference (*20*). This may suggest that counting rates recovered from the myocardium depend on regional myocardial wall thickness in a nonlinear fashion; greater underestimation of regional count change may occur in the thickened myocardial wall. Yamashita et al. (*21*) investigated the %CI of gated myocardial positron emission tomography (PET) compared with the %Th of cardiac magnetic resonance imaging in five normal controls. The two had a good correlation ($r = 0.84$, $y = 0.57 \times +17$), but the %CI tended to be lower than the %Th, especially in the segments

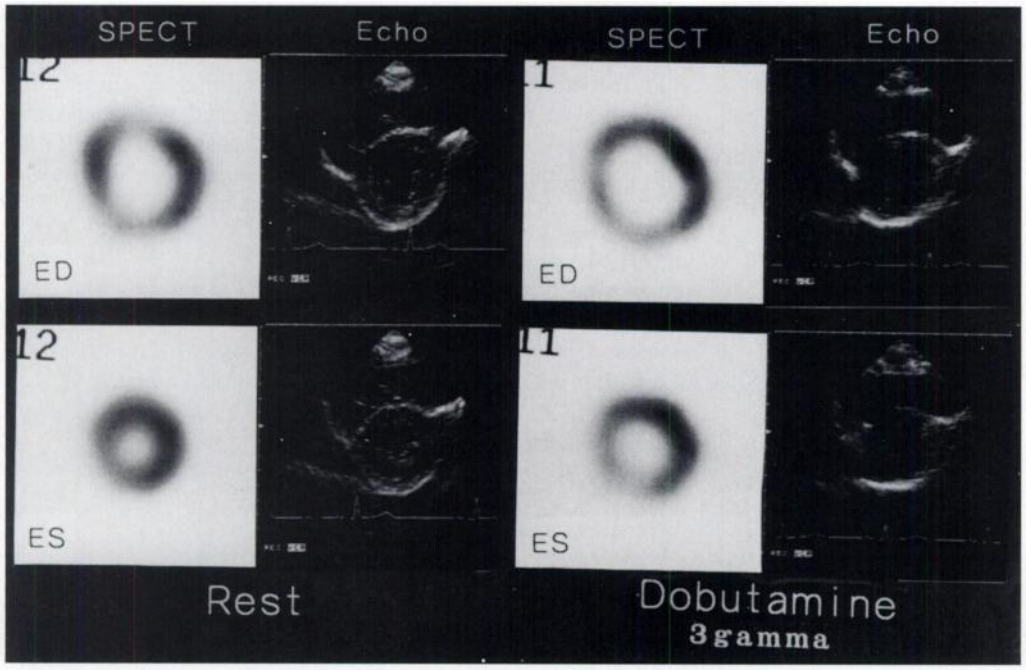

FIGURE 6. Short-axis images of ECG-gated SPECT and echocardiography under rest (left) and 3 μg/kg/min dobutamine infusion (right).

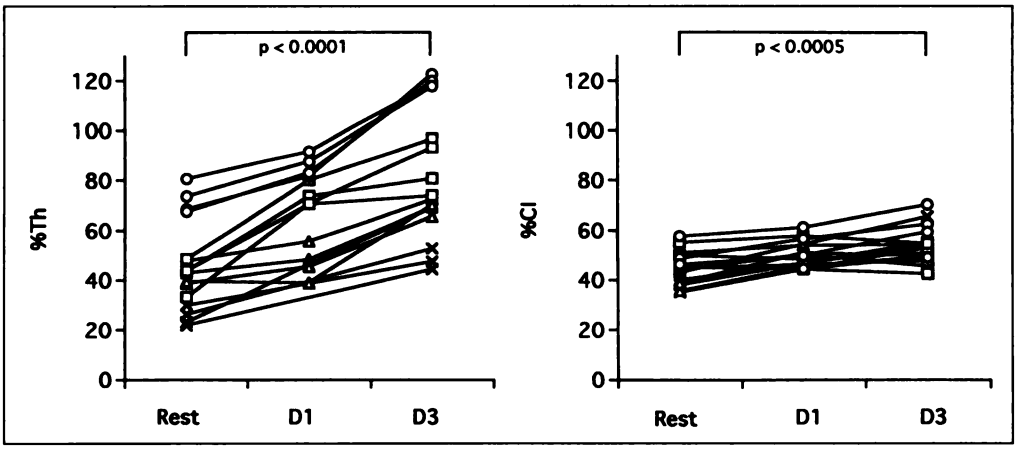

FIGURE 7. Changes of %Th and %CI in each volunteer during dobutamine stress echocardiography (A) and ECG-gated SPECT (B).

where the %Th was high. Our results using SPECT and echocardiography showed the same tendency, but the %CI of ECG-gated SPECT was considerably lower than that of ECG-gated PET of their results. The reason for this underestimation using ECG-gated SPECT is not clear; however, several papers have been presented about the limitations of ECG-gated SPECT for assessment of regional myocardial wall thickening in experimental condition or human studies (*22–24*). Our results are in accord with their ECG-gated SPECT data. In our limited patient population of four normal male volunteers, the %CI resulted in an underestimation of the change in systolic wall thickening. Since our human studies are only for normal volunteers, it is not clear whether we are able to extend these findings to abnormal patients as well. Further investigations in a large patient population are needed for clarification of this point.

The %CI in human data is certainly thought to be dependent on the partial volume effect; however, other unknown factors are also thought to be related. Since ECG-gated SPECT has poor temporal resolution, it may result in underestimation of wall thickening. To avoid this problem, the number of divisions of the R–R interval should be increased, but a relative lengthening of acquisition time is needed. Several investigators have presented the validation of the %CI methods, which are calculated using a model-based estimation or Fourier analysis (*25–27*). Using these methods relatively systolic wall thickening might be calculated, in spite of the small number of frames per cardiac cycle.

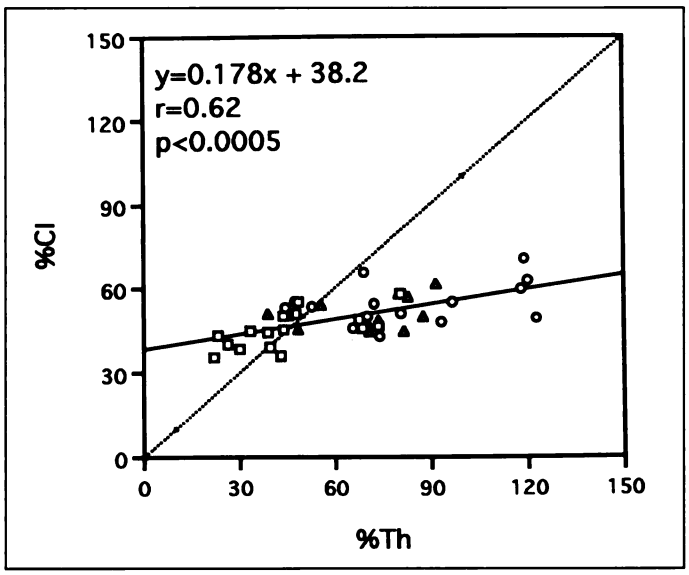

FIGURE 8. Correlation between %CI of ECG-gated SPECT (upper panel) and %Th of echocardiography (lower panel) in 44 segments.

The count density method is based on the hypothesis that regional count density is not changed during the cardiac cycle and that only the object size is changed. Nevertheless, in the myocardium, it is possibile that the vascular space is decreased in the ES phase because of myocardial contraction. If the vascular space were decreased in ES, the regional myocardial tracer concentration would be increased, and the values for %CI might be larger. Further investigations are necessary to resolve this issue.

Other possible limitations of this study concern the accuracy of regional matching of echocardiography and ECG-gated SPECT. Unfortunately, the imaging planes in the two modalities were not identical. There is increasing interest in the correlation of anatomical and functional images of the heart, but it is not matched by experience in thoracic and particularly cardiac studies, whereas registration of multimodal images has become quite common in neurological applications. Comparison with magnetic resonance imaging of the same plane slices, as obtained with SPECT, would be of importance in the further evaluation of this approach.

CONCLUSION

In our phantom studies, the partial volume effect (relationship between count change and wall thickening) was found to be influenced by various conditions in ECG-gated SPECT acquisition. In our preliminary low dose dobutamine infusion study of limited patient population of normal volunteers, the %CI showed an underestimation of regional wall thickening compared with %Th obtained using echocardiography. These data should be considered in the evaluation of the %CI as an index of myocardial function in ECG-gated SPECT.

ACKNOWLEDGMENTS

We thank Yukio Nakamura (Department of Nuclear Medicine, Osaka University Hospital) for his technical assistance and Hyoji Hasegawa (Medical Engineering Laboratory, Toshiba Nasu Works) for his technical support with software programming.

REFERENCES

1. Chua T, Kiat H, Germano G, et al. Gated technetium-99m sestamibi for simultaneous assessment of stress myocardial perfusion, postexercise regional ventricular function and myocardial viability: correlation with echocardiography and rest thallium-201 scintigraphy. *J Am Coll Cardiol* 1994;23:1107–1114.
2. Marcassa C, Marzullo P, Parodi O, Sambuceti G, L'Abbate A. A new method for noninvasive quantitation of segmental myocardial wall thickening using technetium-99m 2-methoxy-isobutyl-isonitrile scintigraphy: results in normal subjects. *J Nucl Med* 1990;31:173–177.
3. Hoffman E, Huang S, Phelps M. Quantitation in positron emission computed tomography: I. Effect of object size. *J Comput Assist Tomogr* 1989;3:299–308.

4. Galt JR, Garcia EV, Robbins WL. Effects of myocardial wall thickness on SPECT quantification. *IEEE Trans Med Imag* 1990;9:144–150.
5. Kahn JK, Henderson EB, Akers AS, et al. Prediction of reversibility of perfusion defects with a single postexercise technetium-99m RP-30A gated tomographic image: the role of residual systolic thickening [Abstract]. *J Am Coll Cardiol* 1988;11:31A.
6. Kumita S, Kumazaki T. Assessment of left ventricular function with ^{99m}Tc-MIBI gated myocardial SPECT using 3 head rotating gamma camera. *Jpn J Nucl Med* 1994;31:43–52.
7. Takeda T, Toyama H, Ishikawa N, et al. Quantitative phase analysis of myocardial wall thickening by technetium-99m 2-methoxy-isobutyl-isonitrile SPECT. *Ann Nucl Med* 1992;6:69–78.
8. Kouris K, Clarke GA, Jarritt PH, Townsend CE, Thomas AN. Physical performance evaluation of the Toshiba GCA-9300A triple-headed system. *J Nucl Med* 1993;34:1778–1789.
9. Ichihara T, Ogawa K, Motomura N, Kubo A, Hashimoto S. Compton scatter compensation using the triple-energy window method for single- and dual-isotope SPECT. *J Nucl Med* 1993;34:2216–2221.
10. National Electrical Manufacturers Association. *NEMA standards publication for performance measurements of scintillation cameras (No. NU1–1980)*, Washington, DC: NEMA; 1980.
11. Garcia EV, Train KV, Maddahi J, et al. Quantification of rotational thallium-201 myocardial tomography. *J Nucl Med* 1985;26:17–26.
12. Klein JL, Garcia EV, DePuey EG, et al. Reversibility bull's-eye: a new polar bull's-eye map to quantify reversibility of stress-induced SPECT thallium-201 myocardial perfusion defects. *J Nucl Med* 1990;31:1240–1246.
13. Akaike H. A new look at the statistical model identification. *IEEE Trans Autom Control* 1974;AC19:716–723.
14. Lieberman AN, Weiss JL, Jugdutt BI, et al. Two-dimensional echocardiography and infarct size: relationship of regional wall motion and thickening to the extent of myocardial infarction in the dog. *Circulation* 1981;63:739–746.
15. Matsuzaki M, Tanaka N, Toma Y, et al. Effect of changing afterload and inotropic states on inner and outer ventricular wall thickening. *Am J Physiol* 1992;263:H109–H116.
16. Mochizuki T, Murase K, Fujiwara Y, Tanada S, Hamamoto K, Tauxe WN. Assessment of systolic thickening with thallium-201 ECG-gated single-photon emission computed tomography: a parameter for local left ventricular function. *J Nucl Med* 1991;32:1496–1500.
17. Weyman AE. *Cross-sectional echocardiography* Philadelphia: Lea & Febiger; 1982: 493–496.
18. Clarke LP, Leong LL, Serafini AN, Tyson IB, Silbiger ML. Quantitative SPECT imaging: influence of object size. *Nucl Med Commun* 1986;7:363–372.
19. Smart SC, Sawada S, Ryan T, et al. Low-dose dobutamine echocardiography detects reversible dysfunction after thrombolytic therapy of acute myocardial infarction. *Circulation* 1993;88:405–415.
20. Kisslo J, von Ramm OT, Thurstone FL. Cardiac imaging using a phased array ultrasound system: II. Clinical technique and application. *Circulation* 1976;53:262–267.
21. Yamashita K, Tamaki N, Yonekura Y, et al. Quantitative analysis of regional wall motion by gated myocardial positron emission tomography: validation and comparison with left ventriculography. *J Nucl Med* 1989;30:1775–1786.
22. Williams KA, Sheridan CM. Regional thickening on gated tomographic polar map Fourier amplitude images as an index of reversible ischemia in severe stress Tc-99m-sestamibi perfusion defects: comparison with resting thallium images [Abstract]. *J Nucl Med* 1996;37:105P.
23. Gradel C, Staib LH, Heller EN, et al. Limitations of ECG-gated SPECT for assessment of regional thickening: experimental comparison with ECG-gated MRI [Abstract]. *J Am Coll Cardiol* 1996;27:241A.
24. Bartlett ML, Buvat I, Vaquero JJ, Mok D, Dilsizian V, Bacharach SL. Measurement of myocardial wall thickening from PET/SPECT images: comparison of two methods. *J Comput Assist Tomogr* 1996;20:473–481.
25. Bacharach SL, Bartlett M, Vaquero JJ, Mok DY, Dilsizian V. Myocardial thickness by gated PET and SPECT: variability and bias [Abstract]. *J Nucl Med* 1993;34(suppl): 178P.
26. Cooke CD, Garcia EV, Folks RD, Ziffer JA. Myocardial thickening and phase analysis from ^{99m}Tc-sestamibi multiple-gated SPECT: development of normal limits [Abstract]. *J Nucl Med* 1992;33:926.
27. Cooke CD, Garcia EV, Cullom SJ, Faber TL, Pettigrew RI. Determining the accuracy of calculating systolic wall thickening using a fast Fourier transform approximation: a simulation study based on canine and patient data. *J Nucl Med* 1994;35:1185–1192.

Significance of Late Redistribution Thallium-201 Imaging after Rest Injection for Detection of Viable Myocardium

Ichiro Matsunari, Susumu Fujino, Junichi Taki, Junji Senma, Takahiko Aoyama, Takanobu Wakasugi, Jun-ichi Hirai, Takashi Saga, Shinichiro Yamamoto and Norihisa Tonami

Departments of Radiology, Cardiology and Cardiovascular Surgery, Fukui Prefectural Hospital, Fukui, Japan; and Department of Nuclear Medicine, Kanazawa University School of Medicine, Kanazawa, Japan

The aim of this study was to determine whether late redistribution imaging after rest injection of ^{201}Tl would provide further information on myocardial viability over conventional rest-early redistribution ^{201}Tl imaging. **Methods:** Twenty-nine patients with coronary artery disease and left ventricular dysfunction underwent rest, early (3–4 hr) and late (20–24 hr) redistribution ^{201}Tl and gated blood pool studies. In 14 patients with successful revascularization, gated blood pool study was repeated after the coronary intervention. **Results:** Nine of 29 patients showed early redistribution, and six additional patients showed further redistribution on the late images. Of 136 segments with initial ^{201}Tl defects, 18 showed early redistribution, and 10 showed late redistribution. When a threshold of 60% of peak activity was used as an index of myocardial viability, only a small fraction (3%) of the initial ^{201}Tl defects were additionally considered viable by the late images. In 14 patients who underwent revascularization, the positive (69%) and negative (87%) predictive values of the early redistribution images for functional recovery were similar to those obtained by the late images (68% and 86%, respectively). **Conclusion:** Although late redistribution after rest injection of ^{201}Tl occasionally occurs, most of the clinically relevant information on myocardial viability may be obtained by conventional rest-early redistribution ^{201}Tl imaging when the defect severity is considered an index of tissue viability.

Key Words: thallium-201; late redistribution; myocardial viability

J Nucl Med 1997; 38:1073–1078

Detection of viable myocardium is an important issue in patients with coronary artery disease (CAD) and left ventricular (LV) dysfunction, in whom coronary revascularization is under consideration (*1,2*). Viable myocardial areas are most likely to benefit from revascularization, whereas revascularization of scarred myocardium will not lead to improvement of LV contractile function. It has been shown that 3- to 4-hr delayed imaging after stress injection of ^{201}Tl frequently underestimates the presence of viable myocardium within persistent defects, as evidenced by improved myocardial perfusion after revascularization (*3*) or by metabolic imaging with [^{18}F]fluorodeoxyglucose and PET (*4,5*). Modified ^{201}Tl protocols, such as late redistribution imaging after stress injection (*6–8*) and reinjection (*9–12*), have been shown to enhance the detection of viable myocardium.

Received Jul. 8, 1996; revision accepted Nov. 23, 1996.

For correspondence or reprints contact: Ichiro Matsunari, MD, Department of Nuclear Medicine, Kanazawa University School of Medicine, 13-1 Takara-machi, Kanazawa, 920 Japan.